# Search for the Rare Decay $B \to K\nu\overline{\nu}$

P. del Amo Sanchez,[1] J. P. Lees,[1] V. Poireau,[1] E. Prencipe,[1] V. Tisserand,[1] J. Garra Tico,[2] E. Grauges,[2]
M. Martinelli[ab],[3] A. Palano[ab],[3] M. Pappagallo[ab],[3] G. Eigen,[4] B. Stugu,[4] L. Sun,[4] M. Battaglia,[5] D. N. Brown,[5]
B. Hooberman,[5] L. T. Kerth,[5] Yu. G. Kolomensky,[5] G. Lynch,[5] I. L. Osipenkov,[5] T. Tanabe,[5] C. M. Hawkes,[6]
A. T. Watson,[6] H. Koch,[7] T. Schroeder,[7] D. J. Asgeirsson,[8] C. Hearty,[8] T. S. Mattison,[8] J. A. McKenna,[8]
A. Khan,[9] A. Randle-Conde,[9] V. E. Blinov,[10] A. R. Buzykaev,[10] V. P. Druzhinin,[10] V. B. Golubev,[10]
A. P. Onuchin,[10] S. I. Serednyakov,[10] Yu. I. Skovpen,[10] E. P. Solodov,[10] K. Yu. Todyshev,[10] A. N. Yushkov,[10]
M. Bondioli,[11] S. Curry,[11] D. Kirkby,[11] A. J. Lankford,[11] M. Mandelkern,[11] E. C. Martin,[11] D. P. Stoker,[11]
H. Atmacan,[12] J. W. Gary,[12] F. Liu,[12] O. Long,[12] G. M. Vitug,[12] C. Campagnari,[13] T. M. Hong,[13] D. Kovalskyi,[13]
J. D. Richman,[13] A. M. Eisner,[14] C. A. Heusch,[14] J. Kroseberg,[14] W. S. Lockman,[14] A. J. Martinez,[14] T. Schalk,[14]
B. A. Schumm,[14] A. Seiden,[14] L. O. Winstrom,[14] C. H. Cheng,[15] D. A. Doll,[15] B. Echenard,[15] D. G. Hitlin,[15]
P. Ongmongkolkul,[15] F. C. Porter,[15] A. Y. Rakitin,[15] R. Andreassen,[16] M. S. Dubrovin,[16] G. Mancinelli,[16]
B. T. Meadows,[16] M. D. Sokoloff,[16] P. C. Bloom,[17] W. T. Ford,[17] A. Gaz,[17] M. Nagel,[17] U. Nauenberg,[17]
J. G. Smith,[17] S. R. Wagner,[17] R. Ayad,[18, *] W. H. Toki,[18] H. Jasper,[19] T. M. Karbach,[19] J. Merkel,[19] A. Petzold,[19]
B. Spaan,[19] K. Wacker,[19] M. J. Kobel,[20] K. R. Schubert,[20] R. Schwierz,[20] D. Bernard,[21] M. Verderi,[21] P. J. Clark,[22]
S. Playfer,[22] J. E. Watson,[22] M. Andreotti[ab],[23] D. Bettoni[a],[23] C. Bozzi[a],[23] R. Calabrese[ab],[23] A. Cecchi[ab],[23]
G. Cibinetto[ab],[23] E. Fioravanti[ab],[23] P. Franchini[ab],[23] E. Luppi[ab],[23] M. Munerato[ab],[23] M. Negrini[ab],[23]
A. Petrella[ab],[23] L. Piemontese[a],[23] R. Baldini-Ferroli,[24] A. Calcaterra,[24] R. de Sangro,[24] G. Finocchiaro,[24]
M. Nicolaci,[24] S. Pacetti,[24] P. Patteri,[24] I. M. Peruzzi,[24, †] M. Piccolo,[24] M. Rama,[24] A. Zallo,[24] R. Contri[ab],[25]
E. Guido[ab],[25] M. Lo Vetere[ab],[25] M. R. Monge[ab],[25] S. Passaggio[a],[25] C. Patrignani[ab],[25] E. Robutti[a],[25] S. Tosi[ab],[25]
B. Bhuyan,[26] V. Prasad,[26] C. L. Lee,[27] M. Morii,[27] A. Adametz,[28] J. Marks,[28] U. Uwer,[28] F. U. Bernlochner,[29]
M. Ebert,[29] H. M. Lacker,[29] T. Lueck,[29] A. Volk,[29] P. D. Dauncey,[30] M. Tibbetts,[30] P. K. Behera,[31] U. Mallik,[31]
C. Chen,[32] J. Cochran,[32] H. B. Crawley,[32] L. Dong,[32] W. T. Meyer,[32] S. Prell,[32] E. I. Rosenberg,[32] A. E. Rubin,[32]
Y. Y. Gao,[33] A. V. Gritsan,[33] Z. J. Guo,[33] N. Arnaud,[34] M. Davier,[34] D. Derkach,[34] J. Firmino da Costa,[34]
G. Grosdidier,[34] F. Le Diberder,[34] A. M. Lutz,[34] B. Malaescu,[34] A. Perez,[34] P. Roudeau,[34] M. H. Schune,[34]
J. Serrano,[34] V. Sordini,[34, ‡] A. Stocchi,[34] L. Wang,[34] G. Wormser,[34] D. J. Lange,[35] D. M. Wright,[35] I. Bingham,[36]
C. A. Chavez,[36] J. P. Coleman,[36] J. R. Fry,[36] E. Gabathuler,[36] R. Gamet,[36] D. E. Hutchcroft,[36] D. J. Payne,[36]
C. Touramanis,[36] A. J. Bevan,[37] F. Di Lodovico,[37] R. Sacco,[37] M. Sigamani,[37] G. Cowan,[38] S. Paramesvaran,[38]
A. C. Wren,[38] D. N. Brown,[39] C. L. Davis,[39] A. G. Denig,[40] M. Fritsch,[40] W. Gradl,[40] A. Hafner,[40] K. E. Alwyn,[41]
D. Bailey,[41] R. J. Barlow,[41] G. Jackson,[41] G. D. Lafferty,[41] T. J. West,[41] J. Anderson,[42] R. Cenci,[42]
A. Jawahery,[42] D. A. Roberts,[42] G. Simi,[42] J. M. Tuggle,[42] C. Dallapiccola,[43] E. Salvati,[43] R. Cowan,[44]
D. Dujmic,[44] P. H. Fisher,[44] G. Sciolla,[44] M. Zhao,[44] D. Lindemann,[45] P. M. Patel,[45] S. H. Robertson,[45]
M. Schram,[45] P. Biassoni[ab],[46] A. Lazzaro[ab],[46] V. Lombardo[a],[46] F. Palombo[ab],[46] S. Stracka[ab],[46] L. Cremaldi,[47]
R. Godang,[47, §] R. Kroeger,[47] P. Sonnek,[47] D. J. Summers,[47] X. Nguyen,[48] M. Simard,[48] P. Taras,[48] G. De
Nardo[ab],[49] D. Monorchio[ab],[49] G. Onorato[ab],[49] C. Sciacca[ab],[49] G. Raven,[50] H. L. Snoek,[50] C. P. Jessop,[51]
K. J. Knoepfel,[51] J. M. LoSecco,[51] W. F. Wang,[51] L. A. Corwin,[52] K. Honscheid,[52] R. Kass,[52] J. P. Morris,[52]
N. L. Blount,[53] J. Brau,[53] R. Frey,[53] O. Igonkina,[53] J. A. Kolb,[53] R. Rahmat,[53] N. B. Sinev,[53] D. Strom,[53]
J. Strube,[53] E. Torrence,[53] G. Castelli[ab],[54] E. Feltresi[ab],[54] N. Gagliardi[ab],[54] M. Margoni[ab],[54] M. Morandin[a],[54]
M. Posocco[a],[54] M. Rotondo[a],[54] F. Simonetto[ab],[54] R. Stroili[ab],[54] E. Ben-Haim,[55] G. R. Bonneaud,[55] H. Briand,[55]
G. Calderini,[55] J. Chauveau,[55] O. Hamon,[55] Ph. Leruste,[55] G. Marchiori,[55] J. Ocariz,[55] J. Prendki,[55] S. Sitt,[55]
M. Biasini[ab],[56] E. Manoni[ab],[56] A. Rossi[ab],[56] C. Angelini[ab],[57] G. Batignani[ab],[57] S. Bettarini[ab],[57] M. Carpinelli[ab],[57, ¶]
G. Casarosa[ab],[57] A. Cervelli[ab],[57] F. Forti[ab],[57] M. A. Giorgi[ab],[57] A. Lusiani[ac],[57] N. Neri[ab],[57] E. Paoloni[ab],[57]
G. Rizzo[ab],[57] J. J. Walsh[a],[57] D. Lopes Pegna,[58] C. Lu,[58] J. Olsen,[58] A. J. S. Smith,[58] A. V. Telnov,[58] F. Anulli[a],[59]
E. Baracchini[ab],[59] G. Cavoto[a],[59] R. Faccini[ab],[59] F. Ferrarotto[a],[59] F. Ferroni[ab],[59] M. Gaspero[ab],[59] L. Li Gioi[a],[59]
M. A. Mazzoni[a],[59] G. Piredda[a],[59] F. Renga[ab],[59] T. Hartmann,[60] T. Leddig,[60] H. Schröder,[60] R. Waldi,[60] T. Adye,[61]
B. Franek,[61] E. O. Olaiya,[61] F. F. Wilson,[61] S. Emery,[62] G. Hamel de Monchenault,[62] G. Vasseur,[62] Ch. Yèche,[62]
M. Zito,[62] M. T. Allen,[63] D. Aston,[63] D. J. Bard,[63] R. Bartoldus,[63] J. F. Benitez,[63] C. Cartaro,[63] M. R. Convery,[63]
J. Dorfan,[63] G. P. Dubois-Felsmann,[63] W. Dunwoodie,[63] R. C. Field,[63] M. Franco Sevilla,[63] B. G. Fulsom,[63]
A. M. Gabareen,[63] M. T. Graham,[63] P. Grenier,[63] C. Hast,[63] W. R. Innes,[63] M. H. Kelsey,[63] H. Kim,[63]

P. Kim,[63] M. L. Kocian,[63] D. W. G. S. Leith,[63] S. Li,[63] B. Lindquist,[63] S. Luitz,[63] V. Luth,[63] H. L. Lynch,[63]
D. B. MacFarlane,[63] H. Marsiske,[63] D. R. Muller,[63] H. Neal,[63] S. Nelson,[63] C. P. O'Grady,[63] I. Ofte,[63]
M. Perl,[63] T. Pulliam,[63] B. N. Ratcliff,[63] A. Roodman,[63] A. A. Salnikov,[63] V. Santoro,[63] R. H. Schindler,[63]
J. Schwiening,[63] A. Snyder,[63] D. Su,[63] M. K. Sullivan,[63] S. Sun,[63] K. Suzuki,[63] J. M. Thompson,[63] J. Va'vra,[63]
A. P. Wagner,[63] M. Weaver,[63] C. A. West,[63] W. J. Wisniewski,[63] M. Wittgen,[63] D. H. Wright,[63] H. W. Wulsin,[63]
A. K. Yarritu,[63] C. C. Young,[63] V. Ziegler,[63] X. R. Chen,[64] W. Park,[64] M. V. Purohit,[64] R. M. White,[64]
J. R. Wilson,[64] S. J. Sekula,[65] M. Bellis,[66] P. R. Burchat,[66] A. J. Edwards,[66] T. S. Miyashita,[66] S. Ahmed,[67]
M. S. Alam,[67] J. A. Ernst,[67] B. Pan,[67] M. A. Saeed,[67] S. B. Zain,[67] N. Guttman,[68] A. Soffer,[68] P. Lund,[69]
S. M. Spanier,[69] R. Eckmann,[70] J. L. Ritchie,[70] A. M. Ruland,[70] C. J. Schilling,[70] R. F. Schwitters,[70]
B. C. Wray,[70] J. M. Izen,[71] X. C. Lou,[71] F. Bianchi[ab],[72] D. Gamba[ab],[72] M. Pelliccioni[ab],[72] M. Bomben[ab],[73]
L. Lanceri[ab],[73] L. Vitale[ab],[73] N. Lopez-March,[74] F. Martinez-Vidal,[74] D. A. Milanes,[74] A. Oyanguren,[74]
J. Albert,[75] Sw. Banerjee,[75] H. H. F. Choi,[75] K. Hamano,[75] G. J. King,[75] R. Kowalewski,[75] M. J. Lewczuk,[75]
I. M. Nugent,[75] J. M. Roney,[75] R. J. Sobie,[75] T. J. Gershon,[76] P. F. Harrison,[76] T. E. Latham,[76] E. M. T. Puccio,[76]
H. R. Band,[77] S. Dasu,[77] K. T. Flood,[77] Y. Pan,[77] R. Prepost,[77] C. O. Vuosalo,[77] and S. L. Wu[77]

(The *BABAR* Collaboration)

[1]*Laboratoire d'Annecy-le-Vieux de Physique des Particules (LAPP),
Université de Savoie, CNRS/IN2P3, F-74941 Annecy-Le-Vieux, France*
[2]*Universitat de Barcelona, Facultat de Fisica, Departament ECM, E-08028 Barcelona, Spain*
[3]*INFN Sezione di Bari[a]; Dipartimento di Fisica, Università di Bari[b], I-70126 Bari, Italy*
[4]*University of Bergen, Institute of Physics, N-5007 Bergen, Norway*
[5]*Lawrence Berkeley National Laboratory and University of California, Berkeley, California 94720, USA*
[6]*University of Birmingham, Birmingham, B15 2TT, United Kingdom*
[7]*Ruhr Universität Bochum, Institut für Experimentalphysik 1, D-44780 Bochum, Germany*
[8]*University of British Columbia, Vancouver, British Columbia, Canada V6T 1Z1*
[9]*Brunel University, Uxbridge, Middlesex UB8 3PH, United Kingdom*
[10]*Budker Institute of Nuclear Physics, Novosibirsk 630090, Russia*
[11]*University of California at Irvine, Irvine, California 92697, USA*
[12]*University of California at Riverside, Riverside, California 92521, USA*
[13]*University of California at Santa Barbara, Santa Barbara, California 93106, USA*
[14]*University of California at Santa Cruz, Institute for Particle Physics, Santa Cruz, California 95064, USA*
[15]*California Institute of Technology, Pasadena, California 91125, USA*
[16]*University of Cincinnati, Cincinnati, Ohio 45221, USA*
[17]*University of Colorado, Boulder, Colorado 80309, USA*
[18]*Colorado State University, Fort Collins, Colorado 80523, USA*
[19]*Technische Universität Dortmund, Fakultät Physik, D-44221 Dortmund, Germany*
[20]*Technische Universität Dresden, Institut für Kern- und Teilchenphysik, D-01062 Dresden, Germany*
[21]*Laboratoire Leprince-Ringuet, CNRS/IN2P3, Ecole Polytechnique, F-91128 Palaiseau, France*
[22]*University of Edinburgh, Edinburgh EH9 3JZ, United Kingdom*
[23]*INFN Sezione di Ferrara[a]; Dipartimento di Fisica, Università di Ferrara[b], I-44100 Ferrara, Italy*
[24]*INFN Laboratori Nazionali di Frascati, I-00044 Frascati, Italy*
[25]*INFN Sezione di Genova[a]; Dipartimento di Fisica, Università di Genova[b], I-16146 Genova, Italy*
[26]*Indian Institute of Technology Guwahati, Guwahati, Assam, 781 039, India*
[27]*Harvard University, Cambridge, Massachusetts 02138, USA*
[28]*Universität Heidelberg, Physikalisches Institut, Philosophenweg 12, D-69120 Heidelberg, Germany*
[29]*Humboldt-Universität zu Berlin, Institut für Physik, Newtonstr. 15, D-12489 Berlin, Germany*
[30]*Imperial College London, London, SW7 2AZ, United Kingdom*
[31]*University of Iowa, Iowa City, Iowa 52242, USA*
[32]*Iowa State University, Ames, Iowa 50011-3160, USA*
[33]*Johns Hopkins University, Baltimore, Maryland 21218, USA*
[34]*Laboratoire de l'Accélérateur Linéaire, IN2P3/CNRS et Université Paris-Sud 11,
Centre Scientifique d'Orsay, B. P. 34, F-91898 Orsay Cedex, France*
[35]*Lawrence Livermore National Laboratory, Livermore, California 94550, USA*
[36]*University of Liverpool, Liverpool L69 7ZE, United Kingdom*
[37]*Queen Mary, University of London, London, E1 4NS, United Kingdom*
[38]*University of London, Royal Holloway and Bedford New College, Egham, Surrey TW20 0EX, United Kingdom*
[39]*University of Louisville, Louisville, Kentucky 40292, USA*
[40]*Johannes Gutenberg-Universität Mainz, Institut für Kernphysik, D-55099 Mainz, Germany*
[41]*University of Manchester, Manchester M13 9PL, United Kingdom*
[42]*University of Maryland, College Park, Maryland 20742, USA*
[43]*University of Massachusetts, Amherst, Massachusetts 01003, USA*

[44]*Massachusetts Institute of Technology, Laboratory for Nuclear Science, Cambridge, Massachusetts 02139, USA*
[45]*McGill University, Montréal, Québec, Canada H3A 2T8*
[46]*INFN Sezione di Milano[a]; Dipartimento di Fisica, Università di Milano[b], I-20133 Milano, Italy*
[47]*University of Mississippi, University, Mississippi 38677, USA*
[48]*Université de Montréal, Physique des Particules, Montréal, Québec, Canada H3C 3J7*
[49]*INFN Sezione di Napoli[a]; Dipartimento di Scienze Fisiche,*
*Università di Napoli Federico II[b], I-80126 Napoli, Italy*
[50]*NIKHEF, National Institute for Nuclear Physics and High Energy Physics, NL-1009 DB Amsterdam, The Netherlands*
[51]*University of Notre Dame, Notre Dame, Indiana 46556, USA*
[52]*Ohio State University, Columbus, Ohio 43210, USA*
[53]*University of Oregon, Eugene, Oregon 97403, USA*
[54]*INFN Sezione di Padova[a]; Dipartimento di Fisica, Università di Padova[b], I-35131 Padova, Italy*
[55]*Laboratoire de Physique Nucléaire et de Hautes Energies,*
*IN2P3/CNRS, Université Pierre et Marie Curie-Paris6,*
*Université Denis Diderot-Paris7, F-75252 Paris, France*
[56]*INFN Sezione di Perugia[a]; Dipartimento di Fisica, Università di Perugia[b], I-06100 Perugia, Italy*
[57]*INFN Sezione di Pisa[a]; Dipartimento di Fisica,*
*Università di Pisa[b]; Scuola Normale Superiore di Pisa[c], I-56127 Pisa, Italy*
[58]*Princeton University, Princeton, New Jersey 08544, USA*
[59]*INFN Sezione di Roma[a]; Dipartimento di Fisica,*
*Università di Roma La Sapienza[b], I-00185 Roma, Italy*
[60]*Universität Rostock, D-18051 Rostock, Germany*
[61]*Rutherford Appleton Laboratory, Chilton, Didcot, Oxon, OX11 0QX, United Kingdom*
[62]*CEA, Irfu, SPP, Centre de Saclay, F-91191 Gif-sur-Yvette, France*
[63]*SLAC National Accelerator Laboratory, Stanford, California 94309 USA*
[64]*University of South Carolina, Columbia, South Carolina 29208, USA*
[65]*Southern Methodist University, Dallas, Texas 75275, USA*
[66]*Stanford University, Stanford, California 94305-4060, USA*
[67]*State University of New York, Albany, New York 12222, USA*
[68]*Tel Aviv University, School of Physics and Astronomy, Tel Aviv, 69978, Israel*
[69]*University of Tennessee, Knoxville, Tennessee 37996, USA*
[70]*University of Texas at Austin, Austin, Texas 78712, USA*
[71]*University of Texas at Dallas, Richardson, Texas 75083, USA*
[72]*INFN Sezione di Torino[a]; Dipartimento di Fisica Sperimentale, Università di Torino[b], I-10125 Torino, Italy*
[73]*INFN Sezione di Trieste[a]; Dipartimento di Fisica, Università di Trieste[b], I-34127 Trieste, Italy*
[74]*IFIC, Universitat de Valencia-CSIC, E-46071 Valencia, Spain*
[75]*University of Victoria, Victoria, British Columbia, Canada V8W 3P6*
[76]*Department of Physics, University of Warwick, Coventry CV4 7AL, United Kingdom*
[77]*University of Wisconsin, Madison, Wisconsin 53706, USA*
(Dated: October 31, 2010)

We present a search for the rare decays $B^+ \to K^+ \nu\overline{\nu}$ and $B^0 \to K^0 \nu\overline{\nu}$ using 459 million $B\overline{B}$ pairs collected with the BABAR detector at the SLAC National Accelerator Laboratory. Flavor-changing neutral-current decays such as these are forbidden at tree level but can occur through one-loop diagrams in the Standard Model (SM), with possible contributions from new physics at the same order. The presence of two neutrinos in the final state makes identification of signal events challenging, so reconstruction in the semileptonic decay channels $B \to D^{(*)} l\nu$ of the $B$ meson recoiling from the signal $B$ is used to suppress backgrounds. We set an upper limit at the 90% confidence level of $1.3 \times 10^{-5}$ on the total branching fraction for $B^+ \to K^+ \nu\overline{\nu}$, and $5.6 \times 10^{-5}$ for $B^0 \to K^0 \nu\overline{\nu}$. We additionally report 90% confidence level upper limits on partial branching fractions in two ranges of di-neutrino mass squared for $B^+ \to K^+ \nu\overline{\nu}$.

PACS numbers: 13.25.Hw, 12.15.-y

———

[*]Now at Temple University, Philadelphia, Pennsylvania 19122, USA
[†]Also with Università di Perugia, Dipartimento di Fisica, Perugia, Italy
[‡]Also with Università di Roma La Sapienza, I-00185 Roma, Italy
[§]Now at University of South Alabama, Mobile, Alabama 36688,

———

USA
[¶]Also with Università di Sassari, Sassari, Italy

The decays $B \to K\nu\overline{\nu}$ arise from flavor-changing neutral currents (FCNC), which are forbidden at tree level in the Standard Model (SM). The lowest-order SM processes contributing to these decays are the $W$ box and the $Z$ penguin diagrams shown in Fig. 1. New physics contributions may enter at the same order as the SM. These contributions, some of which could increase the branching fraction by up to ten times relative to the SM, include: unparticle models [1], Minimal Supersymmetric extension of the Standard Model at large $\tan\beta$ [2], models with a single universal extra dimension [3], scalar Weakly Interacting Massive Particle (WIMP) dark matter [4] and WIMP-less dark matter [5]. A recent SM prediction (ABSW model [6]) for the total $B \to K\nu\overline{\nu}$ branching fraction is $(4.5 \pm 0.7) \times 10^{-6}$, while an earlier prediction (BHI model [7]), based on a different form factor model, is $(3.8^{+1.2}_{-0.6}) \times 10^{-6}$. The BHI model was used by previous analyses [8, 9] and provides a baseline for comparison between results. The current experimental upper limit (UL) on the total branching fraction for $B^+ \to K^+\nu\overline{\nu}$ (charge conjugation is implied throughout) is $1.4 \times 10^{-5}$ at the 90% confidence level (CL) from the Belle Collaboration [8], while an earlier *BABAR* analysis set an UL of $5.2 \times 10^{-5}$ (90% CL) [9]. The only existing UL on the total branching fraction for $B^0 \to K^0\nu\overline{\nu}$ is $1.6 \times 10^{-4}$ (90% CL) from Belle [8].

We report results of a search for $B^+ \to K^+\nu\overline{\nu}$ and $B^0 \to K^0\nu\overline{\nu}$, with branching fractions for both decays as well as for the combination $B \to K\nu\overline{\nu}$. We also report on partial branching fractions for $B^+ \to K^+\nu\overline{\nu}$ in two regions of di-neutrino invariant mass squared ($q^2$). The low-$q^2$ region ($q^2 < 0.4m_B^2$) is selected by requiring $p^*_{K^+} > 1.5\,\mathrm{GeV}/c$ and the high-$q^2$ region ($q^2 > 0.4m_B^2$) by $p^*_{K^+} < 1.5\,\mathrm{GeV}/c$ in the $\Upsilon(4S)$ center-of-mass system (CMS) [10], where $m_B$ is the mass of the $B$ meson and $p^*_{K^+}$ is the magnitude of the CMS 3-momentum of the signal $K^+$ candidate. The high-$q^2$ region is of theoretical interest because the partial branching fraction in this region could be enhanced under some new physics models [6].

This analysis is based on a data sample of $(459.0 \pm 5.1) \times 10^6$ $B\overline{B}$ pairs, corresponding to an integrated luminosity of $\sim 418\,\mathrm{fb}^{-1}$ of $e^+e^-$ colliding-beam data and recorded at the $\Upsilon(4S)$ resonance with the *BABAR* detector [11] at the SLAC PEP-II asymmetric-energy $B$ Fac-

tory. Charged particle tracking is provided by a five-layer silicon vertex tracker and a 40-layer drift chamber in a 1.5 T magnetic field. A CsI(Tl) electromagnetic calorimeter (EMC) is used to measure photon energies and directions and to identify electrons. All quantities in this paper which are measured by the EMC are required to exceed a minimum 20 MeV cluster energy, unless a higher threshold is explicitly noted. The magnetic flux return from the solenoid, instrumented with resistive plate chambers and limited streamer tubes (IFR), provides muon identification. We identify $K^+$ candidates by using a detector of internally reflected Cherenkov light (DIRC) as well as ionization energy loss information from the tracking system.

Due to the presence of two neutrinos in the $B \to K\nu\overline{\nu}$ final state, it is not possible to exploit the kinematic constraints on the $B$ mass and energy which are typically used to distinguish signal and background events in $B$ meson decays at the $\Upsilon(4S)$. Instead, before looking for the signal decay, we first reconstruct a $B$ decay ($B_{\mathrm{rec}}$) in one of several exclusive $D^{(*)}l\nu$ semileptonic final states. We then search for the signal $B \to K\nu\overline{\nu}$ among the remaining charged and neutral particles in the detector that are not part of the $B_{\mathrm{rec}}$. We collectively refer to these remaining particles as $B_{\mathrm{roe}}$ for "rest of the event." This strategy is common to several *BABAR* analyses [12, 13] and has the advantage of higher efficiency compared with reconstruction of the $B_{\mathrm{rec}}$ in hadronic decay modes [9].

We reconstruct the $D$ candidates in the following decay modes: $K^-\pi^+$, $K^-\pi^+\pi^+$, $K^-\pi^+\pi^+\pi^-$, $K^-\pi^+\pi^0$, $K_S^0\pi^+$, and $K_S^0\pi^+\pi^-$. The $K_S^0$ candidates, reconstructed in the $K_S^0 \to \pi^+\pi^-$ mode, are required to have a $\pi^+\pi^-$ invariant mass within $25\,\mathrm{MeV}/c^2$ of the nominal $K_S^0$ mass. $D$ candidates are similarly required to have a reconstructed invariant mass within $60\,\mathrm{MeV}/c^2$ of the nominal value [14], except for the $K^-\pi^+\pi^0$ mode where the range is $100\,\mathrm{MeV}/c^2$. We form $D^{*0} \to D^0\pi^0$, $D^{*+} \to D^0\pi^+$, and $D^{*+} \to D^+\pi^0$ candidates with a required mass difference ($m(D^*) - m(D)$) in the range 130-170 $\mathrm{MeV}/c^2$. In addition, we combine $D$ and $\gamma$ candidates to form $D^*$ candidates with a required mass difference in the range 120-170 $\mathrm{MeV}/c^2$. A $D^{(*)}$ candidate is combined with an identified electron or muon with momentum above 0.8 GeV/c in the CMS to form a $B_{\mathrm{rec}}$ candidate. In events with multiple reconstructed $B_{\mathrm{rec}}$ candidates, we select the candidate with the highest probability that the daughter tracks originate from a common vertex. After a $B_{\mathrm{rec}}$ candidate has been identified, the remaining charged and neutral decay products are used to classify the $B_{\mathrm{roe}}$ as either a background event or a possible signal candidate.

As a first step in refining the selection of $B_{\mathrm{roe}}$ candidates, we veto $K$ candidates which, when combined with a remaining charged or neutral pion candidate, have a $K\pi$ invariant mass within $75\,\mathrm{MeV}/c^2$ of the nominal $K^*(892)$ mass. We also veto events where a remaining charged track can be combined with a $\pi^0$ can-
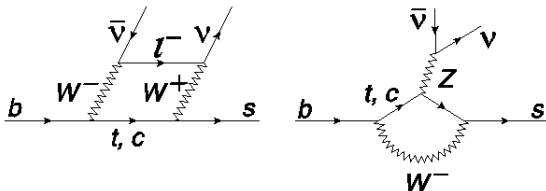


FIG. 1: Lowest-order Feynman diagrams for $B \to K\nu\overline{\nu}$, with the $W$ box on the left and $Z$ penguin on the right.

didate to yield a $\rho^+$ candidate, with a mass window $0.45 < m(\rho^+) < 1.10\,\text{GeV}/c^2$. Similarly vetoed are events where three remaining charged tracks can be combined to yield an $a_1^+$ candidate, with a mass window $0.6 < m(a_1^+) < 2.0\,\text{GeV}/c^2$. These vetoes eliminate, with little loss of signal efficiency, sizable backgrounds that consist mostly of random track combinations. After the vetoes, $B^+$ ($B^0$) signal candidate events are required to possess $K^+$ ($K_s^0 \to \pi^+\pi^-$) candidates, accompanied by at most two (one) additional charged tracks, which are assumed to have been incorrectly left out of the $B_{\text{rec}}$. For the $K^+$ final state, the $B_{\text{rec}}$ lepton daughter and the $K^+$ are also required to be oppositely charged. For the $K_s^0$ final state, signal candidates are required to have a $\pi^+\pi^-$ invariant mass within $25\,\text{MeV}/c^2$ of the nominal $K_s^0$ mass.

At this stage of the selection, each event has a $B_{\text{rec}}$ candidate representing a $B$ meson reconstructed in a semileptonic decay and a $B_{\text{roe}}$ candidate formed from the rest of the event, with the latter representing the signal decay. In simulated $K^+$ ($K_s^0$) signal events that have passed this selection, 99% (92%) of events have a correctly identified signal $K^+$ ($K_s^0$). However, a large background still remains. Further background suppression is achieved using a multivariate event selection algorithm, a bagged decision tree (BDT) [15, 16], that can leverage many weak discriminating variables to achieve high background rejection. Such an algorithm needs to be trained with simulated signal and background events, henceforth referred to as Monte Carlo (MC) events. We use a GEANT4 [17] detector simulation to obtain large samples of simulated signal events generated with a pure phase-space model (which are later re-scaled to the BHI signal model), as well as samples of non-resonant $e^+e^- \to q\bar{q}$ ($q = u,d,s,c$), $B\bar{B}$, and $\tau^+\tau^-$ background events, whose sizes are one ($uds$), two ($c\bar{c}$), three ($B\bar{B}$), and one ($\tau^+\tau^-$) times luminosity. These background events are augmented with a separate sample, with a size 13 times luminosity, of simulated $B\bar{B}$ doubly semileptonic events, the largest source of background.

We construct two ensembles of BDTs, one for the $K^+$ signal mode and one for the $K_s^0$. To create an ensemble, we repeatedly divide the total signal and background datasets in half randomly, creating 20 distinct BDT training and validation datasets, where each dataset has a 50% correlation with any other because approximately 50% of the events are shared. This procedure makes optimal use of the limited statistics of MC events that pass the initial event selection and results in a more statistically precise unbiased estimate of background contributions. Use of the ensemble of 20 BDTs created for each final state also averages out the variations in BDT response compared to a single BDT trained and validated with a single division of the simulated signal and background datasets [18, 19]. The choice of 20 divisions, instead of a lower or higher number, represents a balance between minimizing the variation versus minimizing the overhead of multiple BDTs.

Each BDT of the $K^+$ ($K^0$) ensemble uses 26 (38) dis-

criminating variables, described in the Appendix. These variables fall into four general categories: quantities related to the missing energy in the event, to the overall event properties, to the signal kinematics, and to the overall reconstruction quality of the $B_{\text{rec}}$. Some quantities are given in two different frames and thus allow the BDTs to extract from them additional discriminating power. Several additional variables were initially considered but were pruned during the BDT optimization process, as they were found to add little additional sensitivity.

"Missing Energy" quantities relate to the fact that signal events are expected to possess significant missing energy and momentum because the signal decay includes two neutrinos. In contrast, the dominant background events usually acquire missing energy and momentum as a result of particles passing outside of the detector fiducial acceptance, with the result that distributions of quantities related to missing energy differ between signal and background.

After the $B_{\text{rec}}$ and $K$ or $K_s^0$ signal candidate have been identified, signal events are expected to have little or no additional activity in the detector, other than a few low-energy clusters in the calorimeter resulting from hadronic shower remnants, beam backgrounds, or similar sources. In contrast, background events arising from higher-multiplicity $B$ decays typically possess additional charged or neutral particles within the detector. Variables which characterize this additional detector activity can provide discriminating power between signal and background, and are indicated by the term "extra" in the following.

The strongest discriminant for both $K^+$ and $K^0$ ensembles is $E_{\text{extra}}$, the sum of all detector activity not explicitly associated with either the $B_{\text{rec}}$ or $K$ signal candidate, followed by $p_{K^+}^*$ for the $K^+$ ensemble and by the lab energy of the signal $K_s^0$ for the $K^0$ ensemble. The reconstructed mass of the $D$ from the $B_{\text{rec}}$ is the third ranking variable for both channels.

Figure 2 shows signal, background, and data distributions from the validation set of $K^+$ and $K^0$ BDT output for a BDT randomly selected from the 20 BDTs in the ensemble. The other 19 BDTs are similar to that shown.

We choose as the target signal efficiency the one that maximizes expected signal significance averaged over the 20 BDTs, under the assumption of a branching fraction of $3.8 \times 10^{-6}$. This signal significance is $s/\sqrt{s+b}$, where $s$ is the number of signal events, and $b$ is the number of background events. Optimization using a figure of merit based upon signal efficiency and independent of assumed branching fraction yields similar results. For each BDT, a BDT output value that yields the target signal efficiency is calculated. For example, the BDT output cuts for the BDTs shown in Figure 2 are 0.976 for the $K^+$ BDT and 0.955 for the $K^0$ BDT. The mean background for target signal efficiency is obtained by averaging the individual background estimates from each of the 20 BDTs. Thus, we treat each ensemble of 20 BDTs
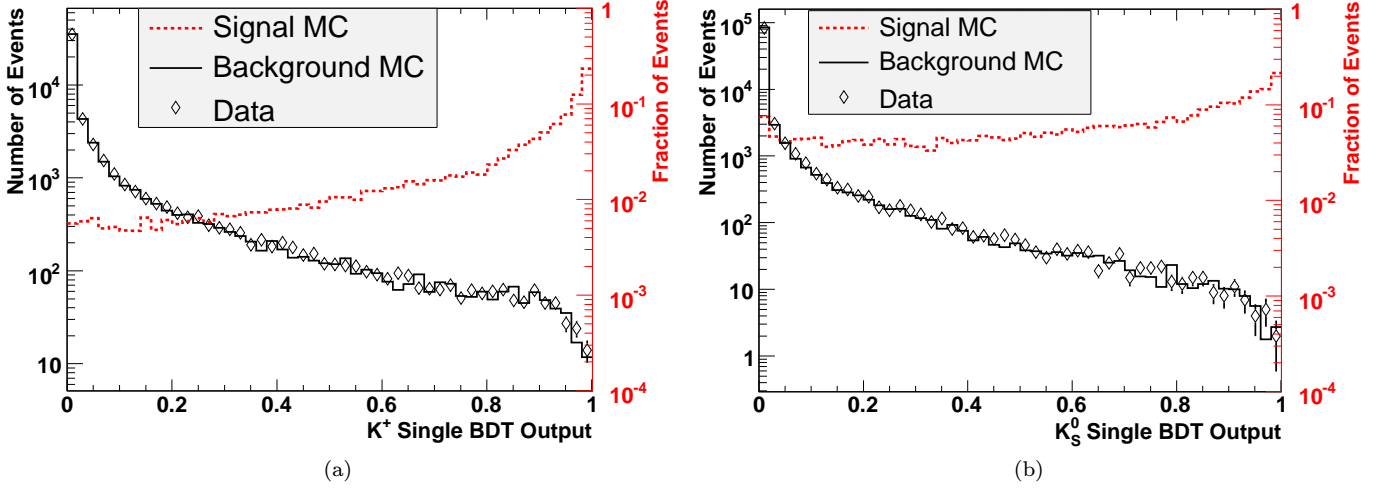
FIG. 2: (a) $K^+$ and (b) $K^0$ BDT output for data (diamonds), background MC (solid), and signal MC (dotted) events. For each plot, the scale for the data and background events is on the left axis, and the scale for the signal events is on the right axis. The distribution of signal MC events is normalized to unit area.

as a set of correlated estimators for the numbers of signal and background events in a signal region defined by the target signal efficiency.

The low-$q^2$ (high-$q^2$) measurement uses the $K^+$ ensemble but only includes events with $p^*_{K^+} > 1.5\,\mathrm{GeV}/c$ ($p^*_{K^+} < 1.5\,\mathrm{GeV}/c$), which means that only those events are used to calculate the signal efficiency and the background prediction. The low-$q^2$ measurement has the same BDT output cuts and background prediction as the primary $K^+$ measurement, with only the signal efficiency changed by the restriction on $p^*_{K^+}$. On the other hand, the high-$q^2$ measurement has its own set of BDT output cuts based upon its own optimized signal efficiency, along with its own background prediction.

The total optimized signal efficiency for the $K^+$ ($K^0$) mode is 0.16% (0.06%), while the efficiency for the $K^+$ low-$q^2$ (high-$q^2$) region is 0.24% (0.28%). The uncertainty in the signal efficiency is discussed below. Figure 3 shows the BDT selection efficiency versus $p^*_K$ for the $K^+, K^0$, and high-$q^2$ measurements, where the BDT selection efficiency considers only the effect of the BDT output cut.

To measure the branching fractions, we use the value obtained from simulated events of the predicted background in the signal region, the number of observed data events, and the signal efficiency, as shown by the following equation: $\mathcal{B} = (N_{obs} - N_{bkg})/\epsilon N_B$, where $\mathcal{B}$ is the branching fraction, $N_{obs}$ is the number of observed data events, $N_{bkg}$ is the number of predicted background events, $\epsilon$ is the total signal efficiency, and $N_B$ is the number of $B$ mesons, either charged or neutral [20], that are relevant to the branching fraction. We account for the 50% correlation between each of the datasets when computing the statistical uncertainty of the estimated

background contribution by using a standard method for combining correlated uncertainties [19].

Data control samples are used to ensure that both signal-like and background-like events in actual data are classified similarly to simulated events. The vetoed $a^+_1$ events offer a high-statistics control sample which can be used to compare the $K^+$ and $K^0$ BDT output distributions for background events in both simulated and actual data. We find good agreement between data and MC events in the BDT output distribution for both final states, with only a $(+5 \pm 2)\%$ data-MC discrepancy. For the $K^+$ mode we make a $+5\%$ adjustment to the expected number of background events, based upon a weighting technique that corrects data-MC discrepancy in the sideband $K^+$ BDT output next to the signal region, and we assign the full adjustment as a systematic uncertainty. Likewise, for the high-$q^2$ $K^+$ measurement, we make a $+25\%$ correction to the expected number of background events and assign the full correction as a systematic uncertainty. In the $K^0_S$ final state, we find a $(+10 \pm 3)\%$ data-MC discrepancy in the sideband BDT output next to the signal region, and we make a $+10\%$ correction and assign the full correction as a systematic uncertainty.

To validate our signal efficiency estimates and assess their systematic uncertainties, we use high-purity samples of $B^+ \rightarrow K^+ J/\psi(\rightarrow \ell^+\ell^-)$ decays (where $\ell^+\ell^- = e^+e^-, \mu^+\mu^-$). The two leptons from the $J/\psi$ are discarded in order to model the unseen neutrinos of the signal decay, and then the events are subjected to the same selection requirements as other signal candidates. Classifying $J/\psi K$ data and MC events, we find only a $(-10 \pm 10)\%$ data-MC discrepancy in the BDT output distribution. Although we do not make any correction, we assign a 10% systematic uncertainty to the
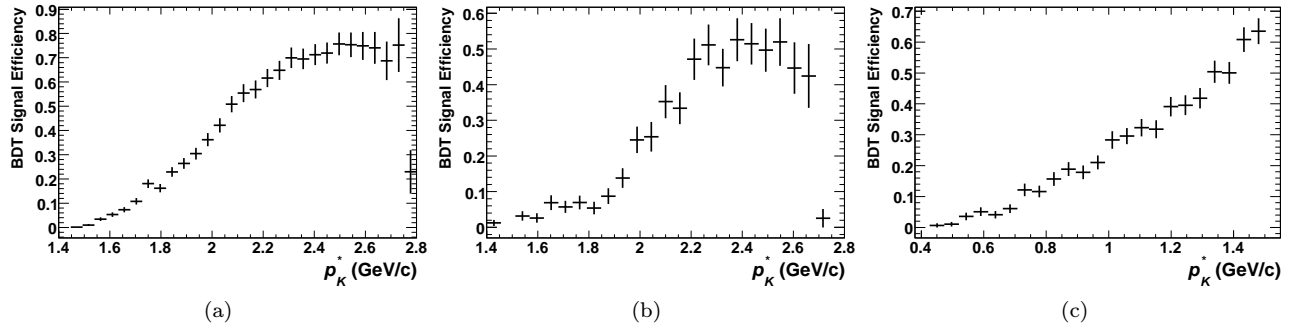
FIG. 3: BDT selection efficiency in the signal region versus $p_K^*$ for (a) $K^+$, (b) $K_S^0$, and (c) high-$q^2$ $K^+$ simulated signal events, considering only the effect of the BDT output cut.

TABLE I: Systematic uncertainties

| Category | Uncertainty |
|---|---|
| Signal efficiency | 14% |
| $K^+$ background prediction | 5% |
| High-$q^2$ $K^+$ background prediction | 25% |
| $K_S^0$ background prediction | 10% |

TABLE II: Total signal efficiencies and MC expectations of the number of data events. The uncertainties shown are systematic for $N_{\text{sgnl}}$, with statistical negligible, and statistical followed by systematic for $N_{\text{bkgd}}$.

| Mode | $\epsilon$ (in %) | $N_{\text{sgnl}}$ | $N_{\text{bkgd}}$ |
|---|---|---|---|
| $K^+$ | 0.16 | $2.9 \pm 0.4$ | $17.6 \pm 2.6 \pm 0.9$ |
| $K_S^0$ | 0.06 | $0.5 \pm 0.1$ | $3.9 \pm 1.3 \pm 0.4$ |
| low-$q^2$ $K^+$ | 0.24 | $2.9 \pm 0.4$ | $17.6 \pm 2.6 \pm 0.9$ |
| high-$q^2$ $K^+$ | 0.28 | $2.1 \pm 0.3$ | $187 \pm 10 \pm 46$ |

TABLE III: Observed and excess data events, with statistical uncertainties [21] shown for $N_{\text{obs}}$ and combined statistical and systematic uncertainties shown for $N_{\text{excess}}$. The last column shows the probability that excess events could be due solely to a background fluctuation.

| Mode | $N_{\text{obs}}$ | $N_{\text{excess}}$ | Prob. |
|---|---|---|---|
| $K^+$ | $19.4^{+4.4}_{-4.4}$ | $1.8^{+6.2}_{-5.1}$ | 38% |
| $K^0$ | $6.1^{+4.0}_{-2.2}$ | $2.2^{+4.1}_{-2.8}$ | 23% |
| low-$q^2$ $K^+$ | $19.4^{+4.4}_{-4.4}$ | $1.8^{+6.2}_{-5.1}$ | 38% |
| high-$q^2$ $K^+$ | $164^{+13}_{-13}$ | $-23^{+49}_{-48}$ | 33% |

TABLE IV: Branching fraction (BF) central values and upper limits. The low- and high-$q^2$ values are partial BFs, while the rest are total BFs.

| Mode | BF $\times 10^{-5}$ | 90% CL $\times 10^{-5}$ | 95% CL $\times 10^{-5}$ |
|---|---|---|---|
| $K^+$ | $0.2^{+0.8}_{-0.7}$ | 1.3 | 1.6 |
| $K^0$ | $1.7^{+3.1}_{-2.1}$ | 5.6 | 6.7 |
| Comb. $K^+, K^0$ | $0.5^{+0.7}_{-0.7}$ | 1.4 | 1.7 |
| Low-$q^2$ $K^+$ | $0.2^{+0.6}_{-0.5}$ | 0.9 | 1.1 |
| High-$q^2$ $K^+$ | $-1.8^{+3.8}_{-3.8}$ | 3.1 | 4.6 |

estimated signal efficiency for all four measurements ($K^+$, $K_S^0$, low-$q^2 K^+$, high-$q^2 K^+$) based on these results. We also assign a signal efficiency systematic uncertainty of 10% to account for the theoretical uncertainties of the signal models. Adding these in quadrature, we assign a total uncertainty of 14% in the estimation of signal efficiency for both final states. Table I summarizes all of the systematic uncertainties.

Table II shows the total signal efficiencies and the expected number of signal and background events in the data. We performed a blind analysis where data events with BDT outputs above the optimized values were not counted or plotted until the analysis methodology and sources of systematic uncertainty were fixed as described above.

Table III shows our results. The non-integer number of observed events results from averaging the integer yields from the 20 BDTs of each type. We calculate two-sided 68% confidence intervals for the number of excess events based on the statistical and systematic uncertainties in the background estimates, as well as the statistical uncertainty on the number of events observed in the data.

Figure 4 shows the averaged BDT outputs in the signal region for $K^+$, $K^0$, and high-$q^2$ $K^+$ data overlaid with the background and signal contributions, while Figure 5 shows similar plots for the $p_K^*$ distribution in the signal region. Figure 6 shows the integrated numbers of events (observed, predicted background, and excess over background) in the signal region for $K^+$, $K^0$, and high-$q^2$ $K^+$ data for each of the 20 BDTs of each type. Table IV gives the branching fraction central values, along with corresponding 90% and 95% CL upper limits, assuming the BHI signal model (the ABSW model gives similar results). The upper limits are calculated using a frequentist method [21]. The quoted uncertainties include all statistical and systematic uncertainties. Our results constrain the $B \to K\nu\bar{\nu}$ branching fraction at the 90% CL to a few times the SM expectation, with limits of $1.3 \times 10^{-5}$ for $B^+ \to K^+\nu\bar{\nu}$ and $5.6 \times 10^{-5}$ for $B^0 \to K^0\nu\bar{\nu}$.
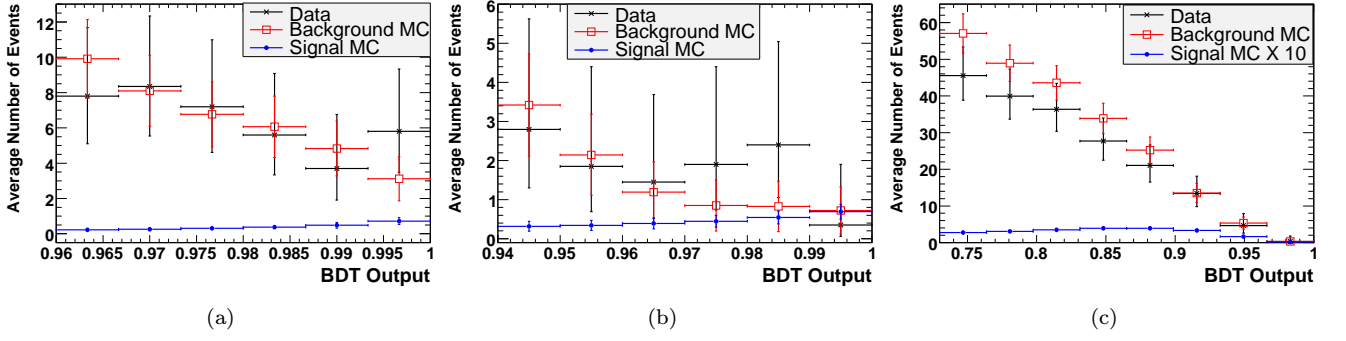
FIG. 4: Averaged BDT signal-region output for (a) $K^+$, (b) $K_S^0$, and (c) high-$q^2$ $K^+$ data, with expected signal and background contributions. The signal estimate assumes a branching fraction of $3.8 \times 10^{-6}$.
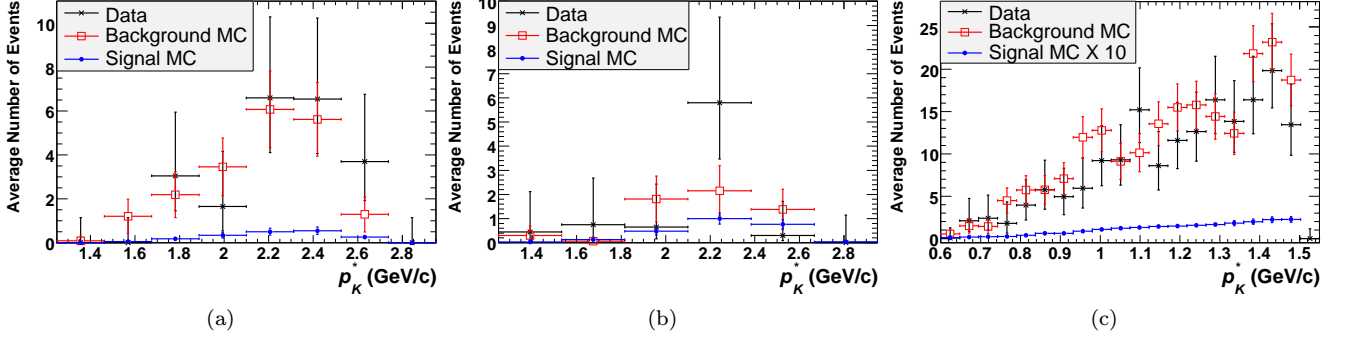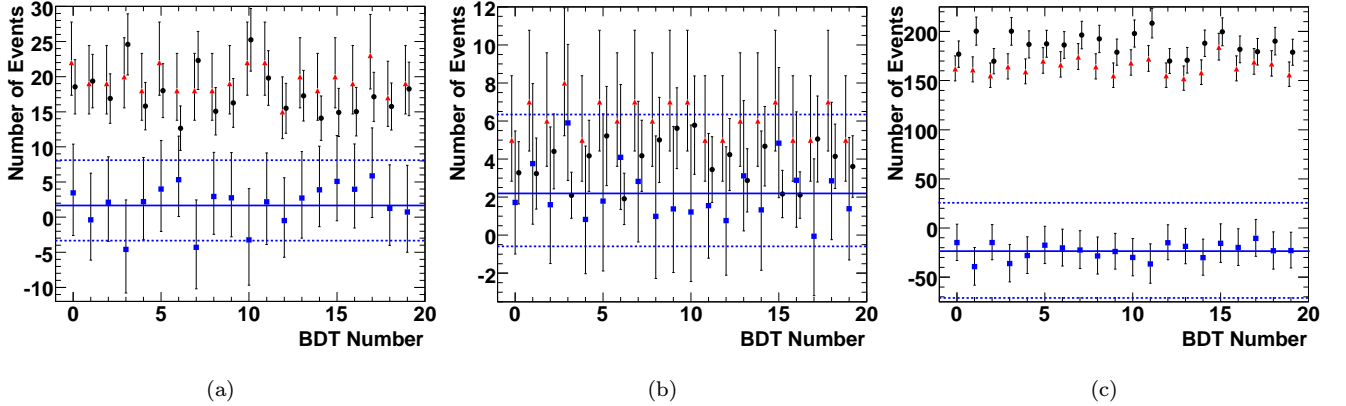


FIG. 5: Averaged $p_K^*$ signal-region output for (a) $K^+$, (b) $K_S^0$, and (c) high-$q^2$ $K^+$ data, with expected signal and background contributions. The signal estimate assumes a branching fraction of $3.8 \times 10^{-6}$.



FIG. 6: Integrated numbers of observed (red triangles), expected background (black circles), and excess events (blue squares) for data for each BDT: (a) $K^+$, (b) $K_S^0$, and (c) high-$q^2$ $K^+$. The individual uncertainties are purely statistical and assume no correlation between data sets. The horizontal dashed lines show the sum of the statistical and systematic uncertainties on the mean number of excess events.

## Appendix

### Definitions of BDT Variables

In the following the notation $[K^+]$ or $[K^0]$ indicates that a variable is used only by that ensemble; otherwise it is used by both BDT ensembles.

BDT input variables related to missing 4-momentum

The event missing 4-momentum is computed from the difference between the 4-momentum of the combined $e^+e^-$ beams and the 4-momenta of all charged and neutral particles reconstructed in the detector.

- Energy component of missing momentum 4-vector

- Energy component of missing momentum 4-vector (CMS)

- Magnitude of the missing momentum 3-vector

- Magnitude of the missing momentum 3-vector (CMS)

- Cosine of the angle with respect to the beam axis of the missing momentum 3-vector

- Cosine of the angle with respect to the beam axis of the 3-momentum vector representing the difference between the initial event momentum and the summed momenta of the $B_{\rm rec}$ and $B_{\rm roe}$ candidates $[K^0]$

BDT input variables related to overall event properties

- $E_{\rm extra} = \Sigma_i E_i$, where $E_i$ is the energy of an isolated EMC cluster or a charged track and the sum is over all tracks or clusters which are not part of the $B_{\rm rec}$ or the $B_{\rm roe}$

- Total energy of all reconstructed charged and neutral particles in the event

- Minimum invariant mass obtained from the combination of any three charged tracks in the event

- Total charge of all tracks in the event $[K^0]$

- Total charge of all tracks matched to EMC energy deposits $[K^0]$

- Number of extra EMC clusters

- Number of $K_L$ candidates in the EMC

- Number of IFR $K_L$ candidates $[K^+]$

- Number of extra reconstructed tracks

- Magnitude of the 3-momentum of a candidate $\Upsilon(4S)$ computed from the $B_{\rm rec}$ and $B_{\rm roe}$ 4-momenta $[K^0]$

- Angle with respect to the beam axis of a candidate $\Upsilon(4S)$ 3-momentum vector computed from the $B_{\rm rec}$ and $B_{\rm roe}$ 4-momenta $[K^0]$

- Normalized second Fox-Wolfram moment of the overall event

BDT input variables related to signal kinematics

- Cosine of the angle between the signal $K$ and the event thrust axis

- Cosine of the angle between the signal $K$ and the $Dl$ thrust axis

- Energy of the signal kaon $[K^0]$

- Reconstructed invariant mass of the signal $K_S^0$ $[K^0]$

- Magnitude of the 3-momentum of the signal kaon

- Magnitude of the CMS 3-momentum of the signal kaon

- Cosine of the angle with respect to the beam axis of the 3-momentum vector of the signal kaon

- Uncertainty in the $x$-component of the signal $K$ point of closest approach to the $e^+e^-$ interaction point, as determined from a three dimensional fit, with the $x$-axis defined perpendicular to the beam axis in the horizontal plane of the detector $[K^0]$

- Uncertainty in the $x$-component of the signal $K$ point of closest approach to the $e^+e^-$ interaction point, as determined by a fit in the $xy$-plane, with the $x$-axis defined perpendicular to the beam axis $(z)$ in the horizontal plane of the detector $[K^0]$

BDT input variables related to $B_{\rm rec}$ reconstruction

- $\chi^2$ per degree of freedom of the vertex fit of the tracks making up the $B_{\rm rec}$

- $\cos\theta_{BY} \equiv (2E^*_{beam} \cdot E^*_{Dl} - m^2_{Bn} - m^2_{Dl})/(2p^*_{Dl} \cdot \sqrt{E^{*2}_{beam} - m^2_{Bn}})$, where $E^*_{beam}$ is one half the total CMS energy, $m_{Bn}$ is the nominal $B$ meson mass [14] and $E^*_{Dl}$, $m_{Dl}$ and $p^*_{Dl}$ are the CMS energy, invariant mass and 3-momentum magnitude of the $D$ - lepton combination used in the reconstruction of the $B_{\rm rec}$

- $\cos\theta_{BY}$ re-calculated with the addition of a photon to the $Dl\nu$ candidate such that $100 < (m(D^0,\gamma) - m(D^0)) < 150\,\mathrm{MeV}/c^2$

- Reconstructed decay mode of the $D$ from the $B_{\mathrm{rec}}$

- Uncertainty in the $x$-component of the point of closest approach to the $e^+e^-$ interaction point of the leading pion daughter from the $D$ meson, with the $x$-axis defined perpendicular to the beam axis in the horizontal plane of the detector

- Number of daughters possessed by the reconstructed $D$ from the $B_{\mathrm{rec}}$

- Number of extra $\pi^0$ candidates satisfying $0.115 < m(\gamma\gamma) < 0.150\,\mathrm{GeV}/c^2$ and $E_\gamma > 30$ MeV

- Reconstructed invariant mass of the $B_{\mathrm{rec}}$

- Reconstructed invariant mass of the $D$ from the $B_{\mathrm{rec}}$

- Magnitude of the CMS 3-momentum of the $B_{\mathrm{rec}}$ $[K^0]$

- Magnitude of the CMS 3-momentum of the $D$ candidate from the $B_{\mathrm{rec}}$

- Magnitude of the 3-momentum of the lepton from the $B_{\mathrm{rec}}$ $[K^0]$

- Magnitude of the CMS 3-momentum of the lepton from the $B_{\mathrm{rec}}$

---

[1] T. M. Aliev, A. S. Cornell and N. Gaur, JHEP **0707**, 072 (2007).

[2] Y. Yamada, Phys. Rev. D **77**, 014025 (2008).

[3] P. Colangelo, F. De Fazio, R. Ferrandes and T. N. Pham, Phys. Rev. D **73**, 115006 (2006).

[4] C. Bird, P. Jackson, R. V. Kowalewski and M. Pospelov, Phys. Rev. Lett. **93**, 201803 (2004).

[5] D. McKeen, Phys. Rev. D **79**, 114001 (2009).

[6] W. Altmannshofer, A. J. Buras, D. M. Straub and M. Wick, JHEP **0904**, 022 (2009).

[7] G. Buchalla, G. Hiller and G. Isidori, Phys. Rev. D **63**, 014015 (2000).

[8] K. F. Chen *et al.* [BELLE Collaboration], Phys. Rev. Lett. **99**, 221802 (2007).

[9] B. Aubert *et al.* [*BABAR* Collaboration], Phys. Rev. Lett. **94**, 101801 (2005).

[10] All kinematic quantities in this paper are defined in the lab frame unless marked with an asterisk, in which case they are in the CMS.

[11] B. Aubert *et al.* [*BABAR* Collaboration], Nucl. Instrum. Meth. A **479**, 1 (2002).

[12] B. Aubert *et al.* [*BABAR* Collaboration], Phys. Rev. D **79**, 091101 (2009).

[13] B. Aubert *et al.* [*BABAR* Collaboration], Phys. Rev. D **76**, 052002 (2007).

[14] C. Amsler *et al.* [Particle Data Group], Physics Letters B, **667**, 1 (2008).

[15] L. Breiman, Mach. Learn. **24**, 2 (1996).

[16] I. Narsky, arXiv:physics/0507157 (2005).

[17] S. Agostinelli *et al.* [GEANT4 Collaboration], Nucl. Instrum. Meth. A **506**, 250 (2003).

[18] B. Efron and R. Tibshirani, *An Introduction to the Bootstrap*, Chapman & Hall (1993).

[19] R. Barlow, *Application of the Bootstrap Resampling Technique to Particle Physics Experiments*, Preprint MAN-HEP-99-4, (2000), www.hep.manchester.ac.uk/preprints/archive.html.

[20] Equal branching fractions for $\Upsilon(4S) \rightarrow B^0\overline{B}^0$ and $\Upsilon(4S) \rightarrow B^+B^-$ are assumed in this paper.

[21] R. Barlow, Computer Physics Communications **149**, 97 (2002).